Investigation of the Heat Transfer Characteristics of a Typical Annular Combustion Chamber of an Industrial Gas Turbine

MARK S. COALMER and KAMBIZ VAFAI

Department of Mechanical Engineering, The Ohio State University, Columbus, Ohio, USA

In the present study a numerical investigation of the heat transfer in an annular combustion chamber of a typical industrial gas turbine was done using a Galerkin-based finite-element solution of the problem. Results were obtained for three basic cases: constant flux incident on the entire combustion segment, constant flux in three quadrants of the chamber and a different magnitude constant flux in the other quadrant, and different magnitude fluxes on the upstream and downstream portions of the chamber. The chamber Biot numbers, dimensionless heat flux, and dimensionless structural wall and thermal barrier coating thicknesses were found to have a crucial effect on the chamber temperature distribution. It was shown that changing the magnitude of the heat flux in a single quadrant prominently alters the temperatures throughout the wall in this area, leading to exceedingly steep temperature gradients. It was also found that any step decrease in downstream incident flux leads to a sharp drop in temperatures at the interface of the thermal barrier coating and the combustion gases.

Industrial gas turbines are utilized worldwide for electrical power generation. Although a plethora of designs are currently being manufactured, most of the designs possess certain common operational features. Ambient air passes through one or more compressor stages, mixes and combusts with fuel gas in a combustion chamber, and powers one or more turbine stages at the chamber outlet. These turbines supply the energy required for the compressor stages, and the remainder of the energy of the combustion gases is used to generate electricity from a power-generating turbine.

Combustion chambers are of three basic types: can, annular, and can-annular [1]. The can type employs individual combustion cans spaced annularly around the engine axis, the annular type is a single chamber consisting of two concentric cylinders coaxial about the engine axis, and the can-annular has characteristics of the can and annular types. The annular chamber makes the best use of space and has the lowest pressure loss, but the large-diameter, thin-walled cylinders often develop structural problems. Large temperature gradients produce high thermal stresses in the chamber walls, and since industrial turbines operate at near capacity for extended periods, thermal fatigue is probable. Therefore, reducing uneven gradients and producing an even temperature distri-

The grant from AMOCO Corporation (no. EES529942) is acknowledged and greatly appreciated.

The present address of Mark S. Coalmer is AMOCO Corporation, Houston, Texas 77253, USA.

Address correspondence to Kambiz Vafai, Department of Mechanical Engineering, The Ohio State University, 206 W. 18th Ave., Columbus, OH 43210-1107.

bution are vital to extending the operating life of the chamber.

The present work yields a clear understanding of the conduction heat transfer characteristics of a typical annular combustion chamber. The study will clarify the effects of material properties, chamber thicknesses, combustion heat production, and air and fuel flow rates on the temperatures of the chamber. Combustion of fuel gas is the source of both radiant heat flux and convection heating for the chamber walls, and cooling air passes along the outside of the walls and into the chamber to reduce the wall temperatures. Typically, fuel enters through multiple, annularly spaced burners and combusts with compressed air to provide an even temperature distribution. However, unequal fuel rates, burner deterioration, and cooling air entering the chamber through multiple ports may result in an uneven temperature distribution. Usually, the total mass flow rate of air from the compressor segment is known, and reasonable estimates are available for the amount of this air that participates in the combustion process. However, downstream of this initial segment, cooling air enters the chamber at flow rates that are not well known. For these reasons, the entrance segment of the chamber and the downstream segment are distinctly different. Therefore, in this work the case of an additional entry point at the midpoint of the chamber as well as the effects of nonuniform radiant heat flux from the combustion process are investigated.

Most annular combustion chamber temperature distributions are obtained by direct measurement, and significant attention has been given to measurement devices and methods [2]. Although methods for estimating wall temperatures exist, the effects of axial and circumferential conduction are often ignored [3]. In the present study a detailed, three-dimensional conduction model of the walls of an annular combustion chamber and the effects of the pertinent parameter variations on the temperature distribution are analyzed.

ANALYSIS

Physical Model and Assumptions

The complexity of the chamber obscures the basic aspects of the pertinent parameters, so the typical chamber geometry was simplified. All of the pertinent aspects of the combustion chamber

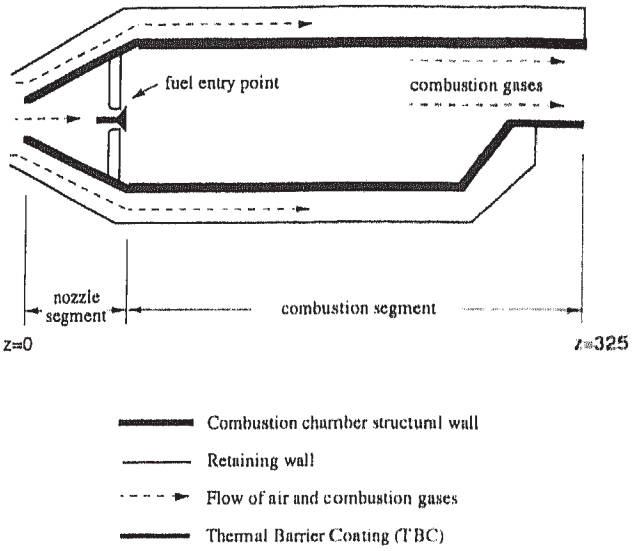

Figure 1 (a) Schematic of a simplified cross section of an annular combustion chamber. (b) Schematic of a simplified half-section of an annular combustion chamber.

are preserved in the simplified typical annular combustion chamber model shown in Figure 1. As shown in this figure, air from the compressor stages is divided into three streams. One stream (typically about 40% of the total mass flow rate) enters the chamber to provide oxygen for combustion. The remaining two streams pass on the outside of the chamber (outside the chamber walls but inside the retaining walls) to cool the chamber walls and enter the chamber downstream to cool the combustion gases. Combustion gases then exit the chamber to power the turbine stages.

The chamber walls, denoted by the thicker lines in Figure 1, usually consist of three materials. In this work the actual material data for a Rolls-Royce industrial gas turbine is used in our simulations. The materials used in this combustion chamber are typical of the materials used in other types of annular combustion chambers. In this case, the nozzle area is made of N75 (80% nickel, 20% chrome), and the combustion area is made of two different materials: C263 (21% chrome, 21% cobalt), and METCO 204B-NS yttria stabilized zirconium thermal barrier coating (TBC), which lines the inside of the combustion area. Thermal conductivity values for these materials were obtained from METCO [4] and from [5].

The combustion of fuel gas is treated as a source of constant radiation heat flux. There is also convective heat transfer to the chamber walls from the combusted gas at 1925°C (3500°F) which flows through the chamber. As mentioned earlier, to investigate the effects of an uneven heat flux

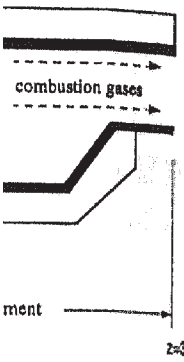

ctural wall

on gases
TBC)

d cross section of an
matic of a simplified
chamber.

d typical annular
vn in Figure 1. As
the compressor
ams. One stream
l mass flow rate)
cygen for combus-
pass on the out-
ne chamber walls
cool the chamber
wnstream to cool
on gases then exit
ie stages.
y the thicker lines
iree materials. In
lata for a Rolls-
sed in our simula-
this combustion
ials used in other
hambers. In this
N75 (80% nickel,
n area is made of
1% chrome, 21%
yttria stabilized
ng (TBC), which
on area. Thermal
aterials were ob-
m [5].
is treated as a
at flux. There is
he chamber walls
C (3500°F) which
ientioned earlier,
uneven heat flux

distribution resulting from an uneven combustion process, the chamber is divided into four quadrants so that as many as four different constant heat fluxes may be imposed simultaneously. The upstream temperature of the chamber walls is assumed to be constant at 390°C (735°F) (as given by Rolls-Royce [6]), and cooling air initially at 390°C (735°F) provides convection cooling outside the chamber walls.

Numerical Methodology

A finite-element method is used to solve the energy equation to obtain the temperature distribution. A simplified analytical solution, among other tests, is used to verify numerical results, and a parametric study affords relations between dimensionless parameter groups and the resulting temperature profiles. This provides an in-depth investigation of various physical heat transfer characteristics of the combustion chamber. The geometry is modeled as a three-dimensional, steady-state conduction problem with no internal heat generation. The governing equation for this problem is given by

$$\frac{\partial}{\partial x^*}\left(k^* \frac{\partial T^*}{\partial x^*}\right) + \frac{\partial}{\partial y^*}\left(k^* \frac{\partial T^*}{\partial y^*}\right) + \frac{\partial}{\partial z^*}\left(k^* \frac{\partial T^*}{\partial z^*}\right) = 0 \tag{1}$$

where the asterisk denotes dimensional quantities. The nondimensional form of the governing equation is more convenient for analysis, so the dimensional variables are scaled with respect to nominal values. The effect of each term is then easily studied by varying one parameter at a time while keeping the other parameters constant. Equation (1) is cast into nondimensional form using the following nondimensional parameter groupings:

$$T = \frac{T_f^* - T^*}{T_f^* - T_0^*} \qquad k = \frac{k^*}{k_c^*} \qquad q = \frac{q^* L_c}{k_c^*\left(T_f^* - T_0^*\right)}$$

$$\mathrm{Bi} = \frac{hL_c}{k_c^*} \qquad x = \frac{x^*}{L_c} \qquad y = \frac{y^*}{L_c} \qquad z = \frac{z^*}{L_c}$$

where the dimensionless temperature T is cast in terms of the wall temperature at the nozzle inlet, T_0^*, and the flame temperature of the fuel gas, T_f^*. Dimensionless temperatures will then vary from zero to one. Thermal conductivity is divided by the (characteristic) conductivity of the TBC, k_c^* $(= k_2)$, to obtain the dimensionless conductivity k. Similarly, the nominal wall thickness is taken as the characteristic length, L_c $(= a_2)$, to create the dimensionless Cartesian coordinates x, y, and z. The Biot number, Bi, is the nondimensional form of the heat transfer coefficient (h), and the dimensionless heat flux, q, is given in terms of the dimensional heat flux, q^*. Equation (1) then takes the form [7]

$$\frac{\partial}{\partial x}\left(k \frac{\partial T}{\partial x}\right) + \frac{\partial}{\partial y}\left(k \frac{\partial T}{\partial y}\right) + \frac{\partial}{\partial z}\left(k \frac{\partial T}{\partial z}\right) = 0 \tag{2}$$

subject to imposed radiative and convective boundary conditions given by

$$q = k \frac{\partial T}{\partial n} \qquad \text{and} \qquad (\mathrm{Bi})T = k \frac{\partial T}{\partial n} \tag{3}$$

To solve Eq. (2) subject to the boundary conditions given by Eq. (3), the Galerkin formulation of the finite-element method (FEM) is used [8]. The domain of interest is divided into small, simply shaped pieces, or elements, which for the present case are trilinear bricks. Within each element the temperature is found using the interpolation functions and the temperatures at the nodal points of that element. The temperature within each element is approximated by

$$T \approx \phi^T [T] \tag{4}$$

where $[T]$ is the column vector of unknown nodal temperatures and ϕ^T is the row vector representing the interpolation function. These approximations are substituted into the governing energy equation to yield a finite set of equations

$$f(\phi, T) = R \tag{5}$$

where R is the error, or residual, that results from the approximation of Eq. (4). The objective of the Galerkin form of the method of weighted residuals is to force the residuals to be orthogonal to the interpolation function, ϕ, and thus reduce the errors to zero. The inner product of orthogonal functions is zero, so the condition may be described as

$$\int_V (f \cdot \phi)\, dV = \int_V (R \cdot \phi)\, dV = 0 \tag{6}$$

where the inner product is defined as the integral over the volume of the element.

For the eight-node brick elements, trilinear interpolation is used to represent the temperature

distribution within each element, and the interpolation function ϕ is defined in terms of the natural coordinates. The derivatives with respect to the physical coordinates are expressed in terms of derivatives with respect to the natural coordinates, and the integral evaluation over the elemental volume is done numerically. The coarsest mesh representation of the chamber consists of approximately 21,100 elements (17,600 nodes); however, a number of cases were run with more than 21,100 elements.

To facilitate interpretation of results, two sets of mesh distributions are used: an inner cylinder set and an outer cylinder set, as in Figure 2. Areas of large temperature gradients are refined to ensure that no significant details are lost. To determine the minimum number of elements required for a precise solution, the temperature of the wall along the inside of the chamber (TBC–combustion gas interface) is plotted in Figure 3 for three

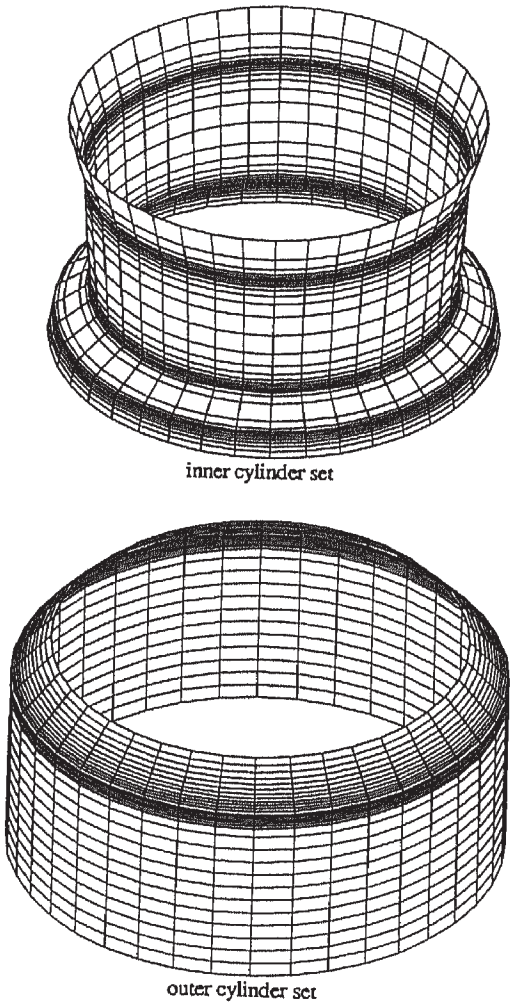

Figure 2 Combustion chamber finite-element mesh displaying inner cylinder set and outer cylinder set.

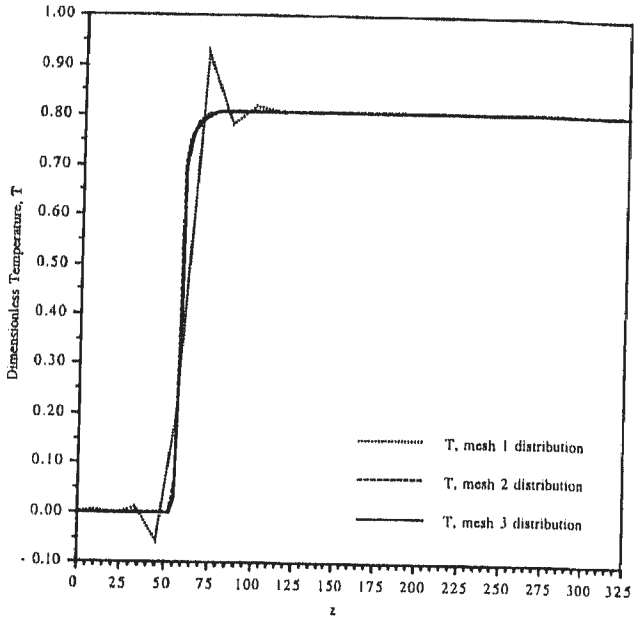

Figure 3 Outer cylinder nondimensional temperature distribution for three FEM mesh representations: mesh 1 = 5,960 elements, ungraded; mesh 2 = 8,880 elements, graded; mesh 3 = 11,360 elements, highly graded.

mesh representations of the outer cylinder. In this figure, mesh 1 is the least refined, and mesh 3, highly graded to increase the number of elements in areas of large temperature difference, is the most refined. As one can see, mesh 2 and mesh 3 temperatures agree, so no further grading or increase in number of elements is required. The same type of result is obtained for the inner cylinder.

As mentioned earlier as part of the verification of the numerical results, a simplified analytical solution is compared with the numerical solution. A right circular cylinder with diameter, wall thickness, and length of the combustion chamber under study is subjected to the following boundary conditions: constant heat flux q_i^* on the inner surface, constant temperature T_o^* on the outer surface, and insulated ends. For this case, the analytical solution can simply be obtained as

$$T^* = \frac{q_i^* r_i^*}{k^*} \ln\left(\frac{r_o^*}{r^*}\right) + T_o^* \tag{7}$$

However, it should be noted that the one-dimensional analytical solution was compared to the full three-dimensional numerical solution of the problem.

For the numerical simulation a coarse 3,744-element mesh and finer 6,912-element mesh were employed to simulate the same right-circular

cylinder described above. The boundary values for the two cases were taken as $q_i^* = 0.00734$ W/m^2 K (150 Btu/s ft^2), $T_o^* = 1{,}095$°C (2,000°F), and $k^* = 5.38 \times 10^{-7}$ W/m K (0.003355 Btu/s ft^2 °F) (the conductivity of N75 at 1,095°C). The results of the two cases are tabulated in Table 1. As can be seen, the percent differences between the analytical solution and the numerical results are almost negligible.

To determine potential anomalies and possible improvements to the design of the combustion chamber, the pertinent input parameters were varied to assess their importance in influencing the heat transfer characteristics of the chamber. A list of these parameters and their corresponding ranges is given in Table 2 for the inner and outer cylinders. Here the thermal conductivities k_1, k_2, and k_3 are for the N75 nozzle area, the C263 combustion area, and the METCO 204B-NS yttria stabilized zirconium thermal barrier coating (TBC), respectively. The parameters a_1 and a_2 represent the nondimensional TBC and chamber wall thicknesses, respectively. These parameters and the boundary conditions for the problem are summarized in Figure 4.

RESULTS AND DISCUSSION

The results for each mesh (inner cylinder and outer cylinder) are given under three categories: equal quadrant heat fluxes, unequal quadrant heat fluxes, and unequal upstream and downstream heat fluxes. In the first category a uniform constant heat flux is assumed over the entire chamber wall in the combustion area. For this case, the quadrant heat fluxes are all set equal to each other. In the second category, these fluxes are not equal to each other. The third category, unequal upstream and downstream heat fluxes, represents the case of cooling air entering the combustion segment at its midpoint to cool the combustion gases. The bulk temperature of the downstream gases is then lower, and thus the net radiation transfer to the downstream chamber walls is also lower. Results are given in the form of dimensionless temperatures plotted as functions of location.

The radiant heat flux is assumed incident on the combustion segment normal to the surface at the interface of the TBC and combustion gases. Figure 5 clarifies the purpose of using a thermal barrier coating. The TBC lowers the temperature of the wall, resulting in improved durability. However, the TBC itself is also susceptible, though to a lesser degree, to high temperatures. Of great importance, then, is also the temperature of the TBC–combustion gas interface of the combustion segment.

Figure 5 represents the results for the nominal case. Temperatures are given along the inner surface (TBC–combustion gas interface), outer surface (structural wall–air interface), and at several intermittent radial locations. No heat flux is imposed upon the relatively low-conductivity nozzle area, so the overall temperature is relatively very low. Conversely, the combustion segment temperatures are relatively high. As expected, the inner surface (TBC–combustion gas interface) exhibits the highest temperature since it is exposed to the direct radiation and convection heating from the combustion process. The low-conductivity TBC results in large temperature gradients in the radial direction, as evidenced by the combustion-segment temperature drop from the TBC–combustion gas interface to the TBC–structural wall interface. The TBC is only three-tenths as thick as the structural wall, but the conductivity of the C263 structural wall (k_2), is 90 times greater than that of the TBC (k_3). Therefore, the temperature drop across the structural wall is relatively small.

To determine the effect of each term in Table 2, one parameter is varied while the others are kept constant at the nominal values. It was found that a change in k_1 does not affect the temperatures of the combustion segment, and a large change in k_1 is required to change the nozzle area

Table 1 Comparison of analytical and numerical (FEM) temperature distributions for a right circular cylinder with diameter, wall thickness, and length of the combustion chamber under study

Radius (ft)	T^*, analytical (°F)	T^*, numerical (3,744 elements) (°F)	Percent Diff. (3,744 elements)	T^*, numerical, (6,912 elements) (°F)	Percent Diff. (6,912 elements)
1.3833	2248.8	2248.0	0.036	2248.5	0.013
1.3840	2219.5	2218.8	0.032	2219.3	0.009
1.3867	2095.0	2094.7	0.014	2094.9	0.005
1.3889	2000.0	2000.0	0.000	2000.0	0.000

Table 2 Range of dimensionless parameters studied for the outer cylinder and inner cylinder

Parameter	k_1	k_2	k_3	Bi_1	Bi_2	Bi_3	Bi_4	q_1	q_2	q_3	q_4	a_1	a_2
Nominal value	16	90	1	3	3	0.8	0.85	1	1	1	1	0.3	1
Outer cylinder minimum value	8	45	0.5	1.5	1.5	0.4	0.425	0.5	0.5	0.5	0.5	0.15	0.5
Inner cylinder minimum value	8	45	0.6	2.4	2.4	0.4	0.425	0.5	0.5	0.5	0.5	0.15	0.5
Outer cylinder maximum value	160	180	2	6	6	1.6	1.7	1.3	1.3	1.3	1.3	0.57	2
Inner cylinder maximum value	160	180	2	6	6	1.6	1.7	1.3	1.3	1.3	1.3	0.51	2

temperature profile noticeably. Even 10 times k_1 only slightly smoothes out the sharp gradient at the beginning of the combustion segment. However, since thermal fatigue occurs at areas of large gradients, a higher-conductivity nozzle material could be beneficial.

Figures 6 and 7 display the results of altering k_2 and k_3, respectively. Taking half of the wall thermal conductivity, k_2, reduces the amount of heat conducted to the outer surface, where it is convected away, and yields a slight increase in the temperatures of the combustion segment. Conversely, doubling k_2 yields a slight temperature decrease. These changes are small due to the fact that the nominal value of k_2 is quite high. Using a higher-thermal-conductivity material has potential to decrease wall temperatures; however, a material that can withstand service temperatures must be selected. Halving and doubling the TBC conductivity, k_3, has similar effects, but since the nominal k_3 is low, the temperature changes are more drastic. Decreasing k_3 raises temperatures, but increasing k_3 lowers them. The maximum temperature decreases from 0.81 for the nominal case to 0.64 for the case of twice the nominal k_3. Also, the large gradient between the nozzle and combustion segments is reduced. The conflict created here is that increasing k_3 allows more heat

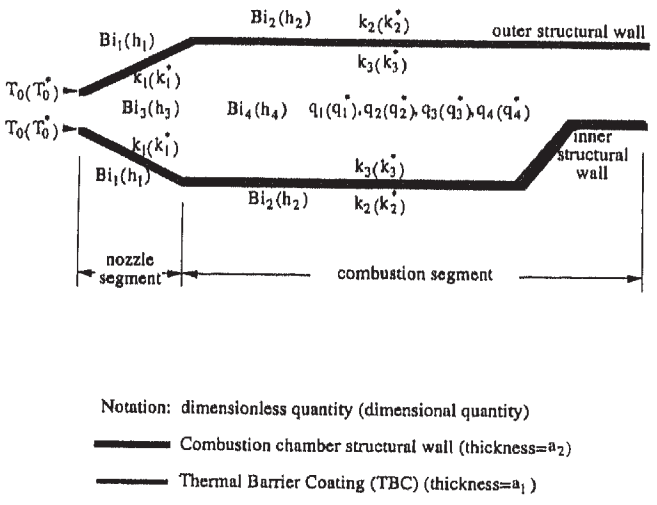

Figure 4 Dimensionless (dimensional) boundary conditions.

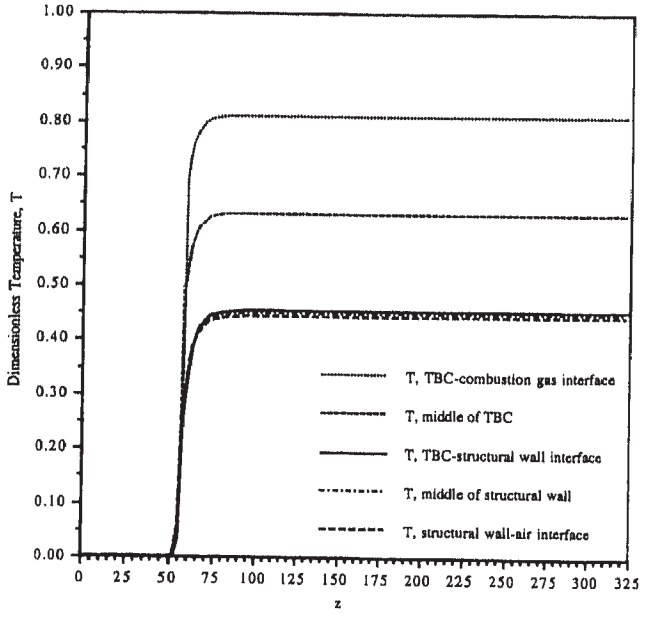

Figure 5 Outer cylinder nominal temperature distribution at several radial locations.

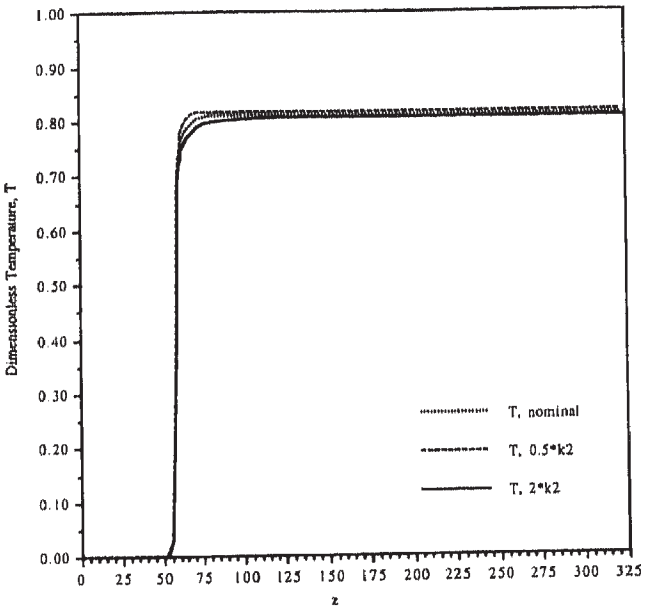

Figure 6 The effect of k_2 on outer cylinder TBC–combustion gas interface temperatures (inside the chamber).

to be conducted to the C263 structural wall, and the limiting temperature for adequate durability may be exceeded. Another consideration is that METCO 204B-NS (TBC) is applied in a thin layer [0.4 mm (0.016 in.) in the present case] by a plasma spray coating process [4] to ensure even coating. Thus a substitute material must also be applicable to the wall surface.

Altering the thicknesses of the TBC and chamber wall is analogous to changing the thermal conductivities. In Figure 8, using 1.9 times the TBC thickness, a_1, is similar to decreasing k_3. Less heat is conducted through the TBC, and the TBC–combustion gas interface temperature increases. Decreasing a_1 has the opposite effect. Since the wall conductivity, k_2, is high, altering the thickness a_2 does not yield significant temperature changes. It should be noted that increasing the structural wall thickness also increases the convective cooling surface area, which results in a decrease in TBC–combustion gas interface temperatures. For the present geometry the decreased conduction effect is greater than the increased convection effect, so the TBC–combustion gas interface temperatures increase.

The Biot numbers govern the amount of cooling that takes place along the outer surface and heating of the inner surface. Magnitudes of these numbers increase with flow velocity, so allowing more cooling air to flow along the outer surface increases Bi_1 and Bi_2. The effects of these parameter changes are shown in Figure 9. Convective cooling is augmented by larger Bi_1 and Bi_2 values, so the inner surface temperature is correspondingly reduced. Smaller values allow higher temperatures, which is undesirable.

The combustion gases on the inside of the chamber are at a higher temperature than the walls, so convective heating occurs. Figure 9 shows that increasing Bi_3 and Bi_4 increases the wall inner surface temperatures. It should be noted

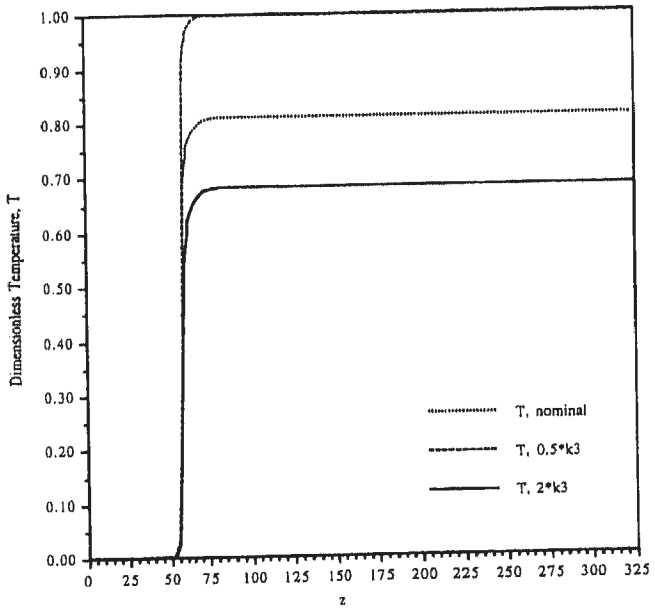

Figure 7 The effect of k_3 on outer cylinder TBC–combustion gas interface temperatures (inside the chamber).

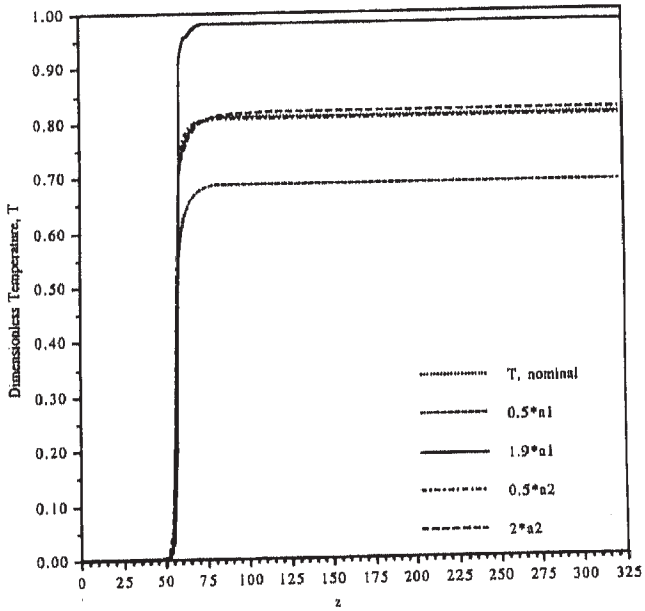

Figure 8 The effect of TBC (a_1) and structural wall (a_2) thicknesses on outer cylinder TBC–combustion gas interface temperatures (inside the chamber).

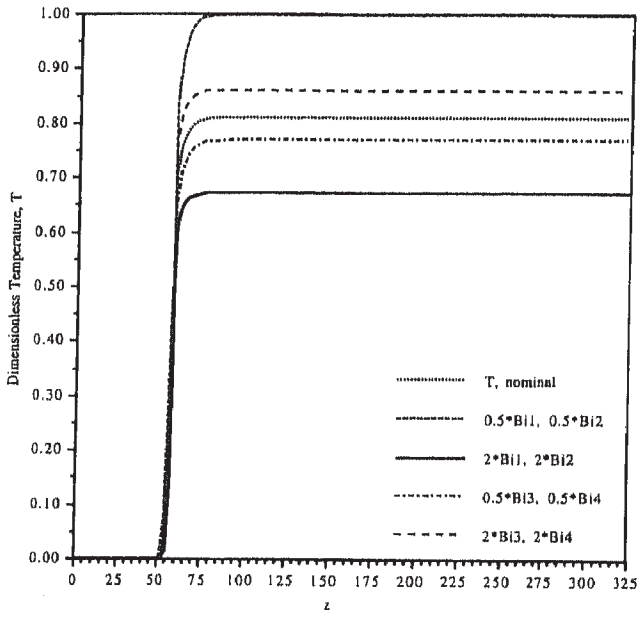

Figure 9 The effect of Biot numbers on outer cylinder TBC–combustion gas interface temperatures (inside the chamber).

that the effects of changing the combustion chamber height can also be deduced from changes in Bi_3 and Bi_4, and the effects of changing the cooling air channel thickness can be deduced from changes in Bi_1 and Bi_2. This is because changes in these dimensions alters the hydraulic diameter, which in effect changes the heat transfer coefficient given by the Dittus-Boelter equation.

Since radiation is the major source of heating, the imposed heat flux affects wall temperatures directly. The magnitude of the imposed heat flux is a consequence of the actual combustion process. High fuel rates, in combination with the required air flow rate, produce more heat than lower fuel and air flow rates. In addition, the air and fuel must be in proper proportion. If more air is supplied than can be utilized (lean mixture), the excess air will absorb heat, and the bulk temperature of the combustion gases will decrease [9]. As a result, the radiation emitted and the convection heating will be less. This tends to reduce inner surface temperatures, but the reduction is partially counterbalanced by the facts that less air is available for cooling and the Biot numbers for convection heating (Bi_3 and Bi_4) are increased. Other factors that alter the amount of radiation incident on the chamber walls include excess fuel (rich mixture), incomplete mixing of air and fuel, and the heat transferred to the surroundings before combustion is complete. The effects of changes in flow rates can be deduced from the results displaying the alterations in Biot numbers.

The present study uses the theoretical combustion temperature (flame temperature) as the bulk temperature of the combustion gases, which does not account for the losses detailed above. All scenarios are covered, however, by the parametric study. Lower combustion gas temperatures decrease convection heating in the chamber, since heating is directly proportional to temperature difference. This information is captured by decreasing Bi_3 and Bi_4, because convection heating is also directly proportional to the Biot number.

Effects of Unequal Quadrant Heat Fluxes

Results obtained from assuming one uniform heat flux value over all four annular quadrants of the chamber provide a base for understanding other chamber scenarios. One such scenario is that the heat flux is constant for each annular quadrant, but that the magnitude can be different in each quadrant. This uneven heat flux situation arises when radiation and/or convection heating vary annularly. Annular variations may result from unequal fuel and/or air distribution from the burners or uneven turbulent mixing of the combustion gases.

Figure 10 shows the effect of the quadrant 1 flux on the TBC–combustion gas interface tem-

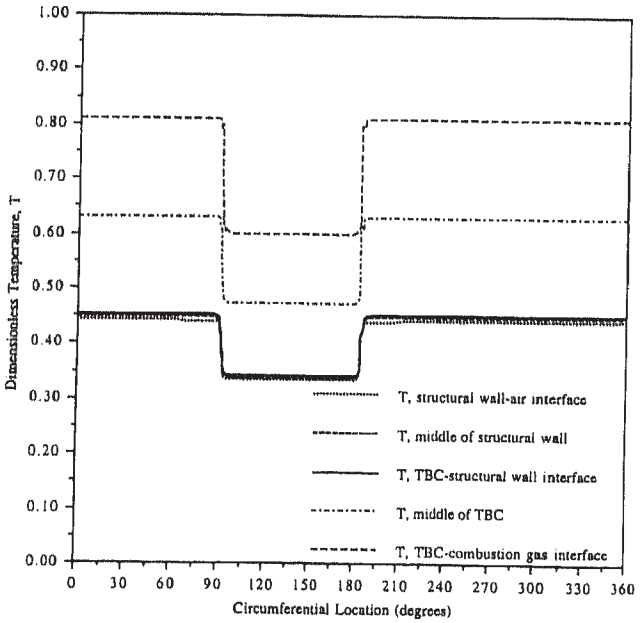

Figure 10 Outer cylinder temperature distribution at several radial locations for q_1 equal to $0.5 * q_1$ (nominal), where q_1 is from 90 to 180° at $z = 200$.

peratures at $z = 200$. The maximum temperatures in quadrants 2, 3, and 4 at each radial location are the same as the nominal case (Figure 5), and the TBC–combustion gas interface temperature in quadrant 1 over the combustion section is reduced. The case where the radiant heat flux in quadrant 1 is doubled follows closely the results presented in Figure 10 except that this time the temperature over quadrant 1 is the maximum temperature.

An important feature in Figure 10 is the creation of a rather sharp gradient where the flux changes. The thermal conductivity of the TBC is so low that even the gradients in the high-conductivity structural wall are steep. Since the chamber is an area of high turbulence and complicated geometry, localized hot spots can easily occur. As seen in Figure 10, areas of concentrated incident flux will not be well conducted to surrounding material. This produces high thermal gradients, resulting in the development of high thermal stresses in both materials.

Effects of Unequal Upstream and Downstream Heat Fluxes

Heat flux may decrease from upstream to downstream due to the introduction of cooling air into the chamber at points along the combustion segment. Since the operating lives of the chamber and turbines are adversely affected by high temperatures, the cooling air is introduced to decrease the bulk temperature of the combustion gases. In general, cooling air can enter at several locations along the structural wall. To understand the important aspects of the cooling air flow patterns, this arrangement is modeled as a single entry point at the midpoint of the combustion segment. This way the basic characteristics of the introduction of the cooling along the combustion segment are better presented.

The introduction of cooling air reduces the bulk temperature of the gases in the chamber, so the incident heat flux is correspondingly reduced. Figure 11 depicts the effects of reduction in the incident flux from $z = 190$ to $z = 325$. The outstanding characteristic seen in Figure 11 is the sharp gradient at the location where flux changes. In addition, it is notable that the temperature varies nearly linearly with the imposed heat flux, which is also true for the case of quadrant flux variations.

At the downstream end the chamber space decreases to channel the flow into the turbine segments, and the geometry of the inner cylinder reflects this. Radiant heat flux is assumed incident on the combustion segment normal to the surface at the interface of the TBC and combustion gases. Figure 12 displays the inner cylinder temperature distribution for the nominal case. Temperatures are given along the outer surface (TBC–combustion gas interface), inner surface (structural wall–air interface), and at several intermittent radial locations. Figure 12 is essentially similar to

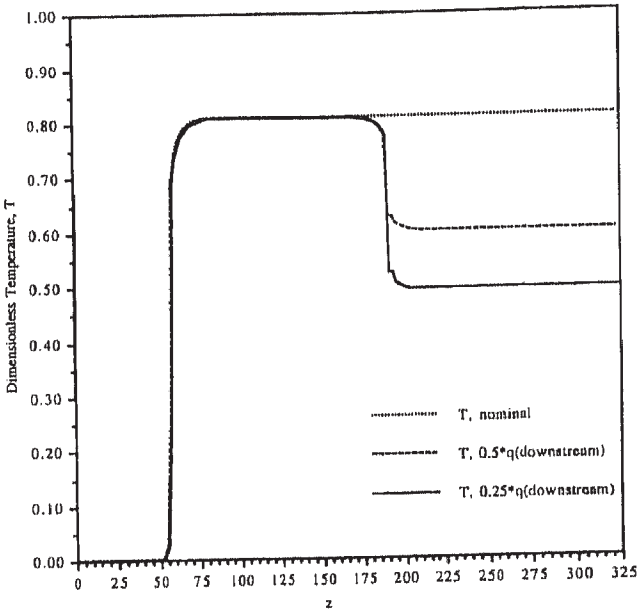

Figure 11 The effect of downstream heat flux on outer cylinder TBC–combustion gas interface temperatures (inside the chamber).

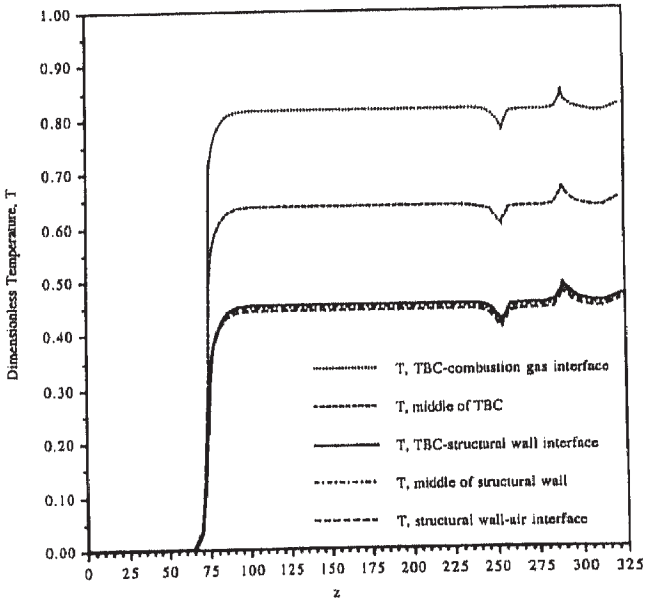

Figure 12 Inner cylinder nominal temperature distribution at several radial locations.

Figure 5, the nominal case for the outer cylinder, except for a small valley and a small peak in each curve at $z = 254$ and $z = 288$, respectively. At $z = 254$ the wall forms angles outward radially, forming a concave shape with respect to the chamber. As a result of this geometry, the amount of material exposed to convective cooling is increased slightly. This results in better heat transfer through the structural material, thus slightly reducing temperature over this region. At $z = 288$, a convex shape is formed and less material is exposed to convective cooling. This results in less heat transfer through the structural material, thus slightly increasing the temperature over this region. Other than the small valley and a small peak in each curve at $z = 254$ and $z = 288$, all other characteristics shown in Figures 6 through 11 remain valid for the inner cylinder.

CONCLUSIONS

The heat transfer characteristics of a typical annular combustion chamber of an industrial gas turbine are studied in the present work. A three-dimensional conduction model of the chamber subject to the convective and imposed radiation heat flux boundary conditions is presented. The numerical results are obtained using a Galerkin-based finite-element method. Biot numbers, dimensionless heat flux, and dimensionless structural wall and thermal barrier coating thicknesses were found to have a crucial effect on the chamber temperature distribution. Results were obtained for three basic cases: constant flux incident on the entire combustion segment, constant flux in three quadrants of the chamber and a different magnitude constant flux in the other quadrant, and different magnitude fluxes on the upstream and downstream portions of the chamber. These cases represented the effects of uneven fuel and/or air distribution from the burners as well as the introduction of cooling air into the chamber for lowering the bulk temperature of the combustion gases.

It was found that, due to the low thermal conductivity of the thermal barrier coating, a steep temperature gradient occurs at the beginning of the combustion segment. A higher value for this thermal conductivity decreases this gradient; however, the temperature of the structural wall may exceed the limiting temperature for adequate durability. A higher-thermal-conductivity nozzle material also reduces this gradient. In addition, it was found that changing the magnitude of the heat flux in a single quadrant prominently alters the temperatures throughout the wall in this area, leading to exceedingly steep temperature gradients. As a result, areas of concentrated incident flux will not be conducted well to surrounding material. High thermal stresses therefore develop in both the thermal barrier coating and the structural wall. Finally, it was shown that any step decrease in incident flux in the flow direction leads to a sharp drop in temperatures at the interface of the thermal barrier coating and the combustion gases.

NOMENCLATURE

a_1	combustion chamber wall thickness, m (ft)
a_2	combustion chamber wall thickness, m (ft)
Bi	Biot number
c	constant
c_p	specific heat at constant pressure
D_e	effective diameter in Dittus-Boelter relation, m (ft)
h	heat transfer coefficient, $W/m^2 K$ ($Btu/s\,ft^2\,°F$)
J	Jacobian matrix
k_1	thermal conductivity of nozzle material, $W/m\,K$ ($Btu/s\,ft\,°F$)
k_2	thermal conductivity of combustion chamber wall, $W/m\,K$ ($Btu/s\,ft\,°F$)
k_3	thermal conductivity of thermal barrier coating, $W/m\,K$ ($Btu/s\,ft\,°F$)
k_a	thermal conductivity of air, $W/m\,K$ ($Btu/s\,ft\,°F$)
k_c	characteristic thermal conductivity, W/mK ($Btu/s\,ft\,°F$)
L_c	characteristic length, m (ft)
n	outward normal to a surface
Pr	Prandtl number
q	thermal radiation heat flux, W/m^2 ($Btu/ft^2\,s$)
$\dot{q}$	volumetric heat generation, W/m^3 ($Btu/ft^3\,s$)
r, θ, z	cylindrical coordinates
R	temperature approximation residual
Re	Reynolds number
t	time, s
T	temperature, °C (°F)
T_f	flame temperature of fuel gas, °C (°F)
T_0	chamber wall temperature at nozzle inlet, °C (°F)

V	volume of a finite element, m^3 (ft^3)
x, y, z	Cartesian coordinates, m (ft)
ξ, η, ζ	natural coordinates of an element
ρ	density, kg/m^3 (lb/ft^3)
ϕ	interpolation function

Superscripts

T	transpose of a matrix

REFERENCES

[1] Treager, I. E., *Aircraft Gas Turbine Technology*, McGraw-Hill, New York, 1979.

[2] Schlader, A. F., Rouiller, P., and Odgers, J., Some Considerations of the Measurement of Temperatures within Aircraft Combustion Chambers, Using a Calorimetric Probe, in *Combustion Heat Transfer in Gas Turbine Systems, Proc. of an Int. Propulsion Symp.*, pp. 363–381, Permagon Press, Oxford, 1971.

[3] Whittaker, M., Theoretical Assessment of Flame Tube Temperatures in a Combustor Operating at Typical S.S.T. Conditions, in *Combustion Heat Transfer in Gas Turbine Systems, Proc. of an Int. Propulsion Symp.*, pp. 183–204, Permagon Press, Oxford, 1971.

[4] METCO Perkin-Elmer, personal communication, 1993.

[5] Raznjevic, K., *Handbook of Thermodynamic Tables and Charts*, Hemisphere, Washington, DC, 1976.

[6] Willbourn, P. M., personal communication, 1993.

[7] Incropera, F. P., and DeWitt, D. P., *Introduction to Heat Transfer*, John Wiley, New York, 1990.

[8] *FIDAP Theoretical Manual*, Fluid Dynamics International, Evanston, IL, 1991.

[9] *North American Combustion Handbook*, North American Manufacturing Company, Cleveland, OH, 1978.

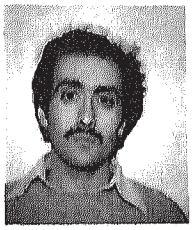

Kamblz Vafai started his bachelor's work in 1972 and acquired his BS in mechanical engineering from the University of Minnesota in 1975. He received his MS (1977) and PhD (1980) in mechanical engineering from the University of California at Berkeley. After spending a year as a postdoctoral fellow at Harvard University, he joined the Ohio State University's department of mechanical engineering in 1981. He was promoted to the rank of full professor in 1991 and became a Fellow of the American Society of Mechanical Engineers in 1992. Dr. Vafai has been an invited visiting professor at the Technical University of Munich in Germany and at the University of Bordeaux in France. Dr. Vafai is the associate editor of the *ASME Journal of Heat Transfer*, and he is also on the editorial board of the *International Journal of Heat and Fluid Flow*. Dr. Vafai has published extensively in the areas of transport through porous media and multiphase transport, natural convection in complex configurations, analysis of porous insulations, high energy storage and recovery, and free surface flows.

Mark S. Coalmer earned a BS in mechanical engineering with distinction in 1992 and an MS in mechanical engineering in 1993, both from The Ohio State University. He now designs oil field fluid handling systems for Amoco Corporation and resides in Houston, Texas.